Tuning of Structural and Magnetic Properties of Nitronyl Nitroxides by the Environment. A Combined Experimental and Computational Study

Carlo Adamo,[†] Andrea di Matteo,[†] Paul Rey[‡], and Vincenzo Barone*[,†]

Dipartimento di Chimica, Universitá "Federico II" via Mezzocannone 4, I-80134 Napoli, Italy, and Laboratoire de Recherche Correspondent du CEA-Grenoble n.7 and Laboratoire de Chimie de Coordination, Service de Chimie Inorganique et Biologique, Dèpartment de Recherche Fondamentale sur la Matière Condensée, CEA-Grenoble, F-38054 Grenoble Cedex 09, France

Received: September 22, 1998; In Final Form: February 23, 1999

The geometry, conformational behavior, and magnetic properties of 2-(2-imidazolyl-)-4,4,5,5-tetramethylimidazoline-1-oxyl-3-oxide, an important spin carrier in molecular magnetic materials, have been studied by a combined experimental and theoretical approach. From the experimental point of view, the avaliable structural data have been completed by new electronic spin resonance spectra in different solvents. From the computational point of view, we have used a hybrid Hartree−Fock/density functional method which provides very reliable structural data. Next, the properties computed at this level have been corrected with reference to refined post Hartree−Fock computations for a smaller model system. Solvent effects have been taken into account by the polarizable continuum model, and crystal field effects have been mimicked by a suitable model cluster. Our computations show that the molecule has a planar structure in the gas phase and in solution, even if the rotational barrier significantly decreases with the polarity of the solvent. In contrast, strong intermolecular hydrogen bonds favor a nonplanar structure in the solid state. As a consequence, a significant modification of the molecular properties is observed going from vacuo to different condensed phases. All of these results are in good agreement with experiments and point out the interpretative power of our integrated computational tool.

1. Introduction

Nitroxides are one of the few classes of organic free radicals that are stable under ordinary physical conditions.[1] This has allowed the determination of a number of molecular structures by using X-ray crystallographic methods and the consequent unequivocal correlation between structural and spectroscopic parameters.[2] This characteristic, coupled with the strong localization of the unpaired spin on the NO moiety,[3] makes nitroxides ideal "spin labels" to explore the structure of short-lived free radicals[4−6] by electron spin resonance (ESR) spectroscopy.[7]

Recently, their use in coordination chemistry has promoted a series of studies devoted to magnetochemistry. Indeed, exceptional stability, ease of chemical modification, and versatility in their coordination properties have made nitroxide free radicals very attractive spin carriers for designing molecular magnetic materials. In particular, nitronyl nitroxides, where the spin density is delocalized onto two sites of coordination, gave molecular networks of various dimensionalities where exchange interactions range from strongly ferro- to strongly antiferromagnetic.[8] The key feature responsible for the properties of such species is the spin density distribution in the nitroxide organic ligands, which tune the magnetic interactions between the different units and may affect even the sign of such interactions.[9] Furthermore, environmental effects, e.g., crystal packing or solute−solvent interactions, significantly influence the spin distribution and, therefore, the magnetic behavior of the radicals[10] and of their metal complexes.

Thus, a better understanding of magnetic properties in metal−organic complexes rests on the evaluation of reliable spin densities in the free organic ligands.[11] In this connection, several studies have shown that methods rooted in the density functional (DF) theory give remarkably accurate results for electronic and magnetic properties of organic radicals.[11−19] In particular, hybrid density functional/Hartree−Fock (DF/HF) approaches are the most effective computational tools.[10,13,20−22] Following this direction, we have recently introduced a "parameter free" hybrid approach,[23,24] which provides even better estimates of magnetic properties.[23,25] Of course, a complete theoretical analysis must include a proper treatment of environmental effects. In this connection, solvent models rooted in the polarizable continuum approach[26] are particularly appealing for the evaluation of solvent shifts on physicochemical properties of open-shell systems.[10,13]

We have recently implemented both of these tools[23,24,27] in the Gaussian series of programs,[28] thus allowing their use in a very effective integrated framework.

On these grounds, and as a first step toward a more detailed analysis of magnetic properties in transition metal−nitroxide complexes, we have studied the geometrical structure and magnetic proprieties of 2-(2-imidazolyl)-4,4,5,5-tetramethylimidazoline-1-oxyl-3-oxide. The interest of this radical rests in the following points: (1) An unusually large intermolecular magnetic coupling transmitted through an H bond is observed in crystals of the pure organic radical.[29] In connection with this fact, a significant influence of the environment on the conformation and magnetic properties is expected. In the crystal structure, a nonplanar arrangement, characterized by a large dihedral angle between the two rings, has been observed. This

* Corresponding author e-mail: enzo@chemna.dichi.unina.it.
[†] Università "Federico II".
[‡] CEA-Grenoble.

10.1021/jp983825s CCC: $18.00
Published on Web 04/17/1999

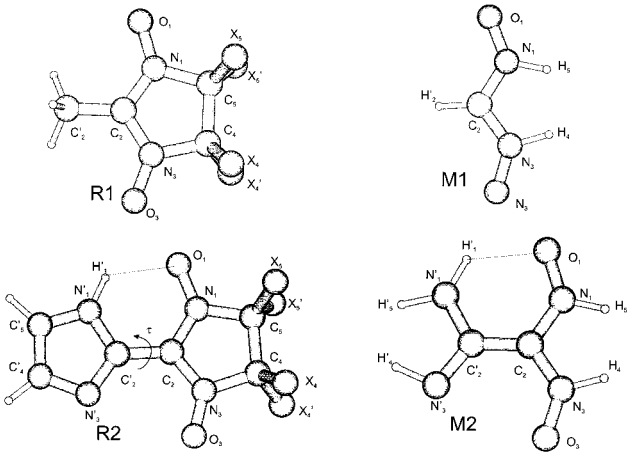

Figure 1. Structure and atom labeling for the nitronyl nitroxide radicals (R1 and R2) and their models (M1 and M2) studied in this work. In the experimental studies, X4, X4′, X5, X5′ are methyl groups, whereas they are hydrogen atoms in quantum mechanical computations.

conformation can be ascribed to intermolecular hydrogen bonding between neighboring imidazole rings.[29] In contrast, intramolecular H bonds should stabilize a planar arrangement. As is well documented, the partial breaking of electron delocalization in π-systems by internal rotations is accompanied by large changes of the electronic and magnetic properties.[30] (2) In the past few years, a number of 0-D, 1-D and 2-D magnetic systems containing this radical and paramagnetic transition metal ions have been synthesized thanks to the bis-chelating nature of the deprotonated radical. These fully characterized magnetic species are possible precursors for three-dimensional ferromagnetic materials where an understanding of the magnetic interactions is not straightforward. Indeed, even in the simplest 0-D complexes three nitroxide ligands are located in close proximity in the coordination sphere of the metal ion[31] and, depending on the sign and magnitude of the different possible interactions, a large variety of magnetic behaviors is expected.

Therefore, a deeper investigation of this nitroxide free radical ligand will bring basic information related to the fast expanding area of both purely organic and metallo-organic magnetic materials.

To the best of our knowledge, the only detailed experimental information available for this molecule concern the solid state,[29] whereas no experimental indications on the conformation of such a molecule in the liquid state are available. We have therefore recorded ESR spectra in different solvents. Comparison of these results with quantum mechanical computations performed for species in vacuo and in consensed phases allows a clear-cut separation between the different effects determining the overall physicochemical behavior. This, in turn, could allow a better understanding of the relationships between molecular structure and spectromagnetic properties. In the same vein, the role of the imidazole ring has been analyzed by a parallel quantum mechanical study of the simplest nitronyl nitroxide radical, which has been used per se as a molecular brick to design molecular-based magnetic materials.[32,33]

2. Computational Details

All of the electronic calculations were carried out with the Gaussian 98 code.[28] In previous works,[23−25] we have shown that reliable molecular properties can be obtained by a family of "parameter-free" DF/HF methods, which mix HF and DF exchange in a fixed ratio. Here we used the so-called B1LYP approach[23] obtained using a mixing of HF and Becke[34]exchange (in a 1:4 ratio) together with the Lee, Yang, and Parr correlation functional.[35] For the purpose of comparison, some computations have been carried out at the unrestricted Hartree−Fock (UHF) level.

The 6-31G(d) basis set[36] has been our standard for all geometry optimizations, while improved magnetic properties were obtained by the EPR-II basis set, which was specifically optimized for computing isotropic hyperfine coupling constants (hcc's).[13,37] Suitable model systems have been investigated using the same basis set and B1LYP geometries also by the coupled cluster method including single and double excitations (CCSD), adding in some cases a perturbative estimate of triple excitations (CCSD[T]).[38] The reliability of this method for organic free radicals is well documented,[39,40] its only drawback being the prohibitive scaling with the number of active electrons.

The hcc's, a_N, are related to the spin densities at the corresponding nuclei by[41]

$$a_N = \frac{8\pi}{3h} g_e \beta_e g_N \beta_N \sum_{\mu,\nu} P^{\alpha-\beta}_{\mu,\nu} \langle \varphi_\mu | \delta(r_{kN}) | \varphi_\nu \rangle \qquad (1)$$

where β_e, β_N are the electron and nuclear magneton, respectively, g_e, g_N are the corresponding magnetogyric ratios, h the Planck constant, $\delta(\mathbf{r})$ is a Dirac delta operator, and $P^{\alpha-\beta}$ is the difference between the density matrixes for electrons with α and β spin occupying the atomic orbitals φ_μ and φ_ν. In the present work, all of the values are given in Gauss (1 G = 0.1 mT), assuming that the free electron g value is appropriate also for the radicals. To convert data to MHz, one has to multiply them by 2.8025.

Solvent effects were evaluated by our implementation of the polarizable continuum model (PCM). In particular, optimized structures and solvation energies have been computed by a cavity model that has been recently introduced and validated,[42] namely the united atoms model for Hartree−Fock (UAHF) computations coupled with the new conductor-like polarizable continuum model (C-PCM).[27b] This approach is strictly related, although not identical, to the so-called COSMO model[27c] and provides results very close to those obtained by the original dielectric PCM[27a] for high dielectric constant solvents, but it is significally more effective in geometry optimizations and is less prone to numerical errors arising from the small part of the solute electron cloud lying outside the cavity (escaped charge effects).[27b,c]

3. Experimental Method and Materials

2-(2-Imidazolyl)-4,4−5,5-tetramethylimidazoline-1-oxyl-3-oxide (R2 in Figure 1) was prepared using a previously reported procedure.[29] ESR spectra were obtained for 0.5 10^{-4} molar solutions of the free radical in the appropriate solvent at room temperature using a Varian E9n X-band spectrometer whose magnetic field was monitored by a Drush NMR gaussmeter. The hyperfine splittings were determined with an accuracy better than 0.03 G.

4. Results and Discussion

The structures and atom numberings of all the radicals considered in the present work are shown in Figure 1. In the radicals studied experimentally, methyl groups are bonded to carbons 4 and 5, but some test computations showed that their replacement with hydrogen atoms has a negligible influence on quantum mechanical results. As a consequence, all of the computations on R1 and R2 have been performed using methylene groups in positions 4 and 5.

TABLE 1: Geometrical Parameters (Distances in Å, Angles in Degrees), Isotropic hcc (*a* in G), and Atomic Spin Populations (n_s) of Nitronyl Nitroxide Radical[a]

	UHF	B1LYP	exptl[b]
N_1-C_2	1.350	1.345	1.335
N_1-O_1	1.246	1.273	1.290
N_1-C_5	1.464	1.487	1.488
C_4-C_5	1.533	1.537	1.540
$N_1-C_2-N_3$	109.4	110.9	107.9
$C_2-N_1-C_5$	112.0	111.2	112.1
$C_2-N_1-O_1$	126.4	127.1	125.0
a (N)	19.8	5.7 (7.5)[c]	|7.6|
a (C_2)	−69.3	−17.4	|12.0|
a (C_5)	−10.3	−4.6	|6.0|
n_s(N)	0.469	0.276	0.257
n_s(O)	0.429	0.349	0.283
n_s(C_2)	−0.800	−0.242	−0.090

[a] All of the geometrical parameters were obtained with the 6-31G(d) basis set, while hcc's and spin population were evaluated by the EPR-II basis set. [b] Geometric parameters from ref 44, isotropic hcc's from ref 47, and spin populations from ref 49. [b] Adding the difference between CCSD[T] and B1LYP values for M2.

It is well-known that one of the most serious drawbacks of unresticted computations on open-shell species is that the resulting wave function is not an eigenstate of S^2 operator. Although the DF approach does not use, in principle, any physically defined wave function, the spin density is evaluated using a reference set of KS orbitals. Under such circumstances the expectation value of S^2 ($\langle S^2 \rangle$) computed for these orbitals should provide a reliable estimate.[43] It is then remarkable that the UB1LYP spin contamination is very low for all the open-shell systems considered in the present study, whereas much higher spin contaminations are obtained by the UHF approach. For instance, for R1 $\langle S^2 \rangle = 0.79$ and 0.92 at the UB1LYP and UHF levels, respectively.

(a) Nitronyl Nitroxide Radical. The ground electronic state of the nitronyl nitroxide radical (R1 hereafter and in Figure 1) has $^2A_2$ symmetry, and the unpaired electron is in an orbital essentially formed by mixing the two π^* orbitals of the N−O moieties with almost equal contributions from the nitrogen and oxygen atoms. Table 1 collects the geometrical parameters of R1, obtained by enforcing a C_{2v} symmetry, together with the available crystallographic data.[44]

There is a good overall agreement between the computed and experimental data. The only significant discrepancy is found for the NO bond, whose computed length is appreciably shorter than the experimental value (1.273 vs 1.290 Å). In view of other experimental and quantum mechanical studies,[45,46] the UB1LYP result seems quite reasonable for isolated nitroxides, so that the experimental value probably reflects the involvement of the nitroxide moieties in intermolecular interactions.

In the same table are reported the computed hcc's, together with the experimental values.[47] It is well-known that the computation of reliable hyperfine structures of nitroxides is particularly demanding,[13,48,49] and also hybrid HF/DF methods do not completely solve this problem. Our results show only a fair agreement with experiments and, in particular, the nitrogen hcc (which plays the most important role in magnetostructural correlations) is underestimated by about 20% (5.7 vs 7.6 G). In a previous work[46] we have shown that accurate isotropic hcc's for nitrogen atoms can be obtained by coupled cluster methods and that, starting from a suitable model compound, the B1LYP approach provides reliable variations due to substituent effects. The difference between coupled cluster and B1LYP isotropic hcc of the nitrogen atoms for the model M1 shown in Figure 1 is 1.8 G. Adding this correction to the nitrogen hcc of R1 computed at the B1LYP level, we obtain a value (7.5 G) in remarkable agreement with experiment (7.6 G).

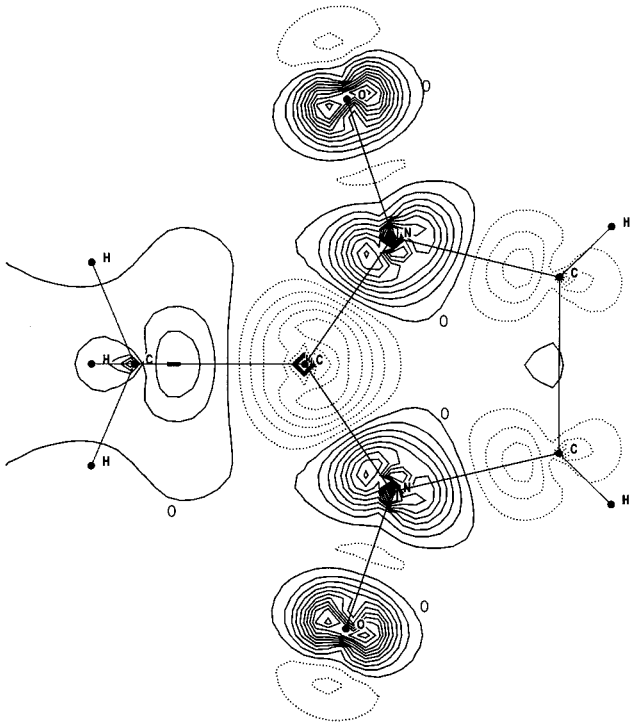

Figure 2. Isospin density plot in the molecular plane of R1. Contour levels are spaced by 0.005 au starting from the absolute minimum on the C_1 atom.

Atomic spin populations (ASPs) for R1 are also reported in Table 1 and are compared to the data obtained in a single-crystal-polarized neutron diffraction investigation on the 4-nitrophenyl substituted analogue.[49] These data indicate that most of the spin density is located on the N and O atoms. Although the UB1LYP ASPs are generally close to the experimental values, a large difference is observed for the C_2 atom, probably arising from an overestimation of spin polarization (vide infra). Note, however, that this effect is attenuated when a phenyl group is bonded to this atom.[11] These results are quite satisfactory taking into account the assumptions made both in quantum mechanical computations and in the elaboration of the experimental data. Furthermore, it must be pointed out that also in this connection HF and MP2 approaches provide quite poor results.[49] Thus the B1LYP approach (possibly corrected by a priori shifts) provides structural, electronic, and magnetic data in fair agreement with the experimental findings for R1. This gives us further confidence about its use for the study of more complex nitronyl nitroxide radicals.

It is also interesting to analyze the overall pattern of the spin density represented in Figure 2, which is qualitatively the same by all of the computational models.

Because the SOMO is concentrated on N and O atoms, their spin populations are quite large and positive (spin delocalization (SD) effect). However, a not negligible negative spin population is found on C2, essentially originating from the so-called spin polarization (SP) effect. The SP contribution is due to the fact that the unpaired electron (by convention with α spin) interacts differently with the electrons of a spin-paired bond, because the exchange interaction (which reduces the Coulomb repulsion) is operative only between electrons with parallel spins. This induces a localization of α-spin density in the σ orbitals of atoms on which the SOMO is localized and a corresponding localization of β-spin density in the σ orbitals of atoms to which they

TABLE 2: Geometric Parameters (Distances in Å, Angles in Degrees) of 2-(imidazole-2-yl)-4,4,5,5-tetramethyl-imidazoline-1-oxyl-3-oxide[a]

geometrical parameters	UHF	B1LYP	exptl[b]
$C_2-C'_2$	1.433	1.439	1.457
C_2-N_3	1.368	1.365	1.341
C_2-N_1	1.355	1.354	1.339
N_1-O_1	1.252	1.285	1.285
N_3-O_3	1.243	1.264	1.283
$C'_2-N'_3$	1.313	1.329	1.319
$C'_2-N'_1$	1.350	1.374	1.345
$N'_1-H'_1$	1.001	1.018	1.001
$O_1-H'_1$	2.113	1.980	2.980
$C'_4-N'_3$	1.355	1.364	1.354
$C'_5-N'_1$	1.361	1.355	1.355
N_1-C_5	1.482	1.480	1.507
N_3-C_4	1.463	1.489	1.493
$N_1-C_2-N_3$	108.6	110.1	109.1
$O_1-N_1-C_2$	126.7	127.4	125.0
$O_3-N_3-C_2$	127.5	128.3	126.5
$C'_2-C_2-N_3$	127.6	126.8	125.2
$C'_2-C_2-N_1$	124.0	123.1	125.6
$N'_3-C'_2-C_2$	126.3	128.0	124.7
$N'_1-C'_2-C_2$	122.2	120.1	123.9
$H'_1-N'_1-C'_2$	124.2	121.8	134.0
$N'_1-C'_2-N'_3$	111.5	111.7	111.3
$C'_4-N'_3-C'_2$	105.4	104.7	105.1
$C'_5-N'_1-C'_2$	106.8	106.0	107.6
$C_4-N_3-C_2$	111.9	110.8	112.3
$C_5-N_1-C_2$	112.6	111.9	112.2
τ	0.0	0.0	48.4

[a] All of the values are computed using the 6-31G(d) basis set. [b] From ref 29.

are directly bonded. This leads, in turn, to accumulation of β-spin density in the π-orbitals of these atoms, and so on. In summary, SP induces a damped oscillatory pattern of spin densities along bonds starting from atoms on which the SOMO is concentrated. In the present case, the effect is especially significant on C2, which receives contributions by both NO groups and has, as a consequence, a quite large negative (β) spin population.

(b) 2-(Imidazole-2-yl)-4,4,5,5-tetramethylimidazoline-1-oxyl-3-oxide radical (R2). The geometry of R2 (see Figure 1) has been fully optimized both at the UB1LYP and UHF levels, with the only limitation of replacing the methyl groups bonded to C4 and C5 by hydrogen atoms. The optimized parameters are collected in Table 2, together with the available crystallographic structure,[29,50] while the atom numbering is reported in Figure 1.

The experimental data indicate a small distortion of the two rings from planarity, probably owing to the presence in the unitary cell of four different molecules that are statistically disordered.[29] The most significant geometrical feature is, anyway, the large dihedral angle between the two rings (τ in Figure 1), which is equal, in the crystal, to 48.4°. This large dihedral angle has been ascribed to the effect of intermolecular hydrogen bonding between the hydrogen of the imidazole ring and $N_{3'}$ of an adjacent imidazole ring, the $N_{1'}$-$N_{3'}$ distance being only 2.87 Å.[29] In contrast, both UHF and UB1LYP computations predict a planar arrangement. As a consequence, the ground electronic state of R2 has A''_2 symmetry, and the unpaired electron is in an orbital which is very similar to the SOMO of R1.

The general trend of the geometrical parameters is the same for the two computational models and suggests that significant geometry distortions occur for the planar conformation. The

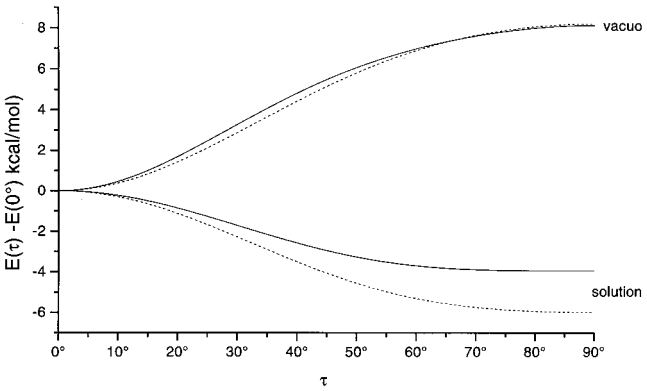

Figure 3. In vacuo torsional curves and solvation free energies for R2 computed at the UB1LYP (continuous lines) and UHF (broken lines) levels.

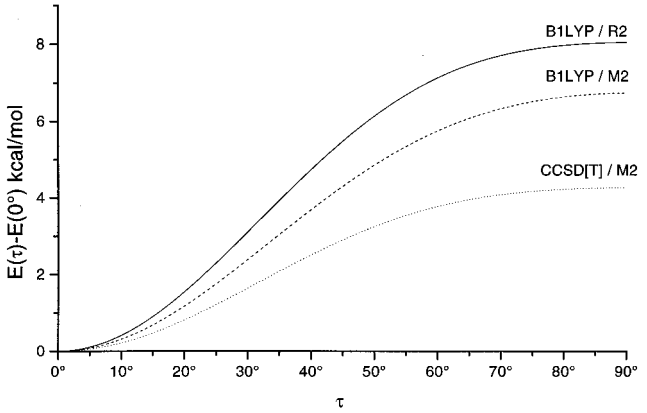

Figure 4. Torsional curves for M2 computed at the B1LYP and CCSD-[T] levels and for R2 at the B1LYP level.

UB1LYP values are, as expected, closer to experimental data than the UHF values. This does not occur, of course, for those parameters which are significantly affected by the conformation of the molecule, e.g., bond lengths and valence angles in the inter-ring region, where the planar disposition of the system induces values that are larger than experimental findings.

This apparent discrepancy between experimental and theoretical indications induced us to analyze in deeper detail the conformational behavior of R2. To this end, we have performed calculations at the UB1LYP level, evaluating the minimum energy geometries at selected values of the inter-ring dihedral angle τ (flexible rotor model, FRM). The potential energy profiles computed in the gas phase are plotted in Figure 3.

Both UHF and UB1LYP computations predict an energy minimum for $\tau = 0°$ and a significant barrier for the conformation at $\tau = 90°$ (8.2 and 8.1 kcal/mol, respectively). However, we think that both methods overestimate the stability of the planar conformation, although for different reasons. On one hand, the B1LYP functional correctly reproduces hydrogen bonds, but like all of the other DF approaches overestimates conjugation effects;[30] on the other hand, the HF method has exactly the opposite characteristics. On these grounds, we resorted to a composite approach in which the low-level (DF) results for the actual system are corrected by the difference between the results of low-level and high-level (here CCSD-(T)/6-31G*) computations on suitable model compounds. In particular, single point B1LYP and CCSD(T) computations have been performed for M2 (see Figure 1) using the geometrical parameters optimized for R2 (except for CH bond lengths which are constrained to 1.09 Å). The curves shown in Figure 4 indicate that M2 and R2 have similar conformational charac-

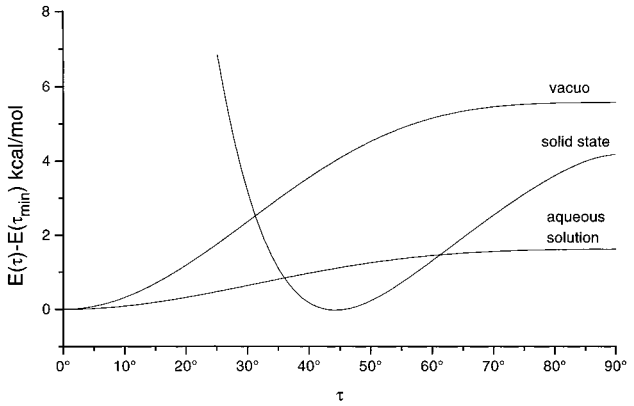

Figure 5. Improved B1LYP torsional curves for R2 in vacuo and in condensed phases.

teristics and that, as anticipated, the B1LYP torsional barrier is overestimated.

The potential $E(\tau)$ governing variations of the τ angle can be described by the leading terms of the Fourier expansion[51]

$$\Delta E(\tau) = E(\tau) - E(0°) = {}^1/_2 \sum V_j (1 - \cos j\tau)$$

and symmetry requirements forbid odd values of j. Furthermore, as previously found for similar systems,[51] our computations show that a remarkable fit both of UHF and UB1LYP energies is obtained by

$$\Delta E(\tau) = {}^1/_2 [V_2 (1 - \cos 2\tau) + V_4(1 - \cos 4\tau)]$$

so that

$$E(90°) - E(0°) = V_2$$

As a consequence, just two computations at a more refined level are sufficient to correct the V_2 value obtained at the B1LYP level. For the model compound, the whole $E(\tau)$ obtained scaling the V_2 term in the B1LYP results is very close to that obtained by CCSD[T] computations, thus suggesting that the V_4 term obtained at the UB1LYP level is essentially correct. This confirms that the UB1LYP method is just overestimating conjugation energies E_c between both rings, which, as is well-known,[51] are well approximated by

$$\Delta E_c(\tau) = P^2(\pi)_{ir}\, \beta(\pi)_{ir}\, (1 - \cos 2\tau)$$

thus affecting only the V_2 term of the Fourier expansion. In the above equation, $P(\pi)_{ir}$ and $\beta(\pi)_{ir}$ are the density and Fock matrix elements governing π interactions between inter-ring atoms (C_2 and $C_{2'}$) in planar conformations. Because the σ contribution to inter-ring bonding is essentially independent of τ and on the nature of further substituents of C_{ir} atoms, we can write

$$\Delta E_c(\tau) = kP^2(\text{tot})\, (1 - \cos 2\tau)$$

where P(tot) is the total bond order between C_{ir} atoms (computed by a Mulliken population analysis) and k is a constant which can be determined once forever by refined computations on model compounds

$$k = [\Delta E(90°)_{hl} - \Delta E(90°)_{ll}]/P^2(\text{tot})_{ll}$$

where *ll* and *hl* stand, respectively, for low and high level of computation. Using this correction we end up with the scaled torsional curves of R2 shown in Figure 5, where the most stable conformation remains planar, but the torsional barrier is reduced to 5 kcal/mol.

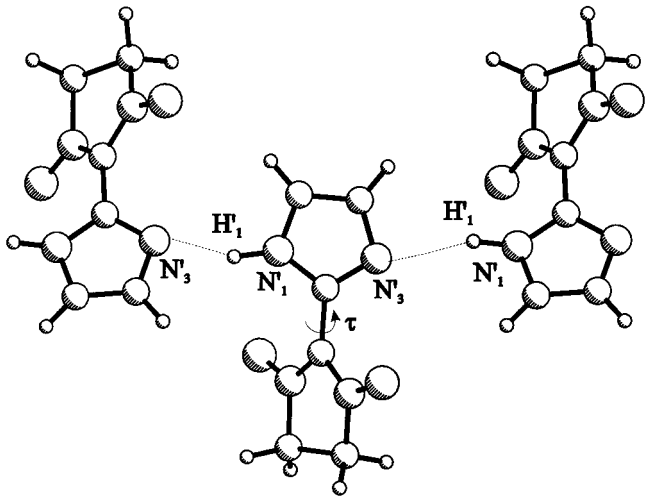

Figure 6. Cluster used to represent short-range intermolecular interactions in the crystal of R2.

The strength of the intramolecular H bond may be significantly affected by interactions with surrounding solvent molecules. So, we have computed the modifications induced in the torsional potential of R2 by bulk solvent. From a quantitative point of view, we have repeatedly shown that solvent effects are well reproduced by the PCM/DF approach, so that an improved torsional curve can be obtained by adding to our best results in vacuo solvation energies obtained at the same geometries by the B1LYP/C−PCM model. Although UHF computations give similar trends (Figure 3), they overestimate, as usual, electrostatic solvent effects due to the preference of ionic resonance forms obtained at the UHF level both in vacuo and in solution. It is remarkable that the solvation free energy has a trend opposite to that of the intrinsic torsional energy in that twisted structures are now preferred with respect to the planar minimum obtained in vacuo. Competition between both effects leads to a planar equilibrium structure also in solution, but to a torsional barrier continuously decreasing with the dielectric constant of the solvent (by about 4 kcal/mol in water, at the UB1LYP level). Note that the larger solvation energy of twisted structures is simply related to their higher dipole moment. As a matter of fact the dipole moment increases from 3.86 to 4.45 D when going from $\tau = 0°$ to $\tau = 90°$.

The role played by the competition between intramolecular H-bonds and interactions with the environment on the conformational behavior of R2 is also evident in the crystal structure, where, as already mentioned, a nonplanar arrangement has been found.[29,46] However, the crystal is formed by "clusters" of three R2 moieties involved in intermolecular hydrogen bridges, and the steric hindrance connected with this structure could significantly alter the conformational behavior of free R2. To better clarify this point, we have modeled the cluster by considering a system formed by one molecule of R2 H-bonded to two molecules of imidazole. The whole cluster is depicted in Figure 6.

For nitronyl nitroxide and imidazole rings we have used the geometrical structure optimized at the B1LYP level, whereas intermolecular parameters have been taken from the crystallographic study.[50] Although this is only a simple model of the crystal structure, we think that it retains the essential features leading to competition between intra- and intermolecular H bonds in determining the conformational behavior of R2 in the crystal.

TABLE 3: Isotropic hcc (in Gauss) of R2 Obtained by Different Methods both in Vacuum and in Solution[a]

atom	B1LYP (vacuum)	B1LYP PCM	B1LYP $4H_2O$	B1LYP PCM + $4H_2O$	exptl[b] water
C'_2	5.0	4.7	4.3	4.5	
N'_3	−0.9	−0.8	−0.7	−0.7	
N'_1	−0.4	−0.5	−0.4	−0.5	
C'_5	−1.8	−1.0	−1.5	−0.9	
C'_4	1.8	1.0	1.0	0.9	
C_2	−17.0	−17.9	−17.2	−18.1	
H'_1	0.7	0.7	0.7	0.7	
N_1	6.4	6.8	6.7	7.3	7.9
N_3	5.3	6.2	6.1	7.1	7.9
C_5	−4.5	−4.5	−4.7	−4.8	
C_4	−4.9	−4.8	−5.4	−5.2	
O_1	−10.2	−10.2	−10.0	−10.6	
O_3	−12.5	−12.4	−12.9	−12.6	

[a] All values have been obtained by the EPR-II basis set. [b] The corresponding values in CH_2Cl_2 are 7.4 G.

Next, we have evaluated the torsional energy profile around the τ dihedral angle at the UB1LYP level, freezing bond lengths and valence angles at their equilibrium values (rigid rotor model, RRM). The resulting curve (corrected as described above) is plotted in Figure 6. The energy minimum is found now at $\tau = 43°$, in remarkable agreement with the experimental value in the solid state ($\tau = 48.4°$).

In summary, our theoretical analysis sheds some light on the different behavior of R2 in different condensed phases. In the absence of environmental constraints, i.e., in the gas phase, R2 has a planar arrangement, with a high barrier restricting the rotation around the $C_2-C_{2'}$ bond. This barrier significantly decreases in aqueous solution because the H-bond strength is weakend by solute−solvent interactions. Finally, a nonplanar arrangement is found in the solid state because of strong and specific intermolecular H bonds with neighboring molecules.

There is, of course, a direct relationship between the molecular structure and the ESR spectra of R2. Table 3 compares the experimental data with the hcc's computed at the B1LYP level both in vacuo and in solution.

As already mentioned, most of the spin density is located on the NO groups in a π^* orbital similar to the SOMO of R1. The molecular plane is the nodal plane of the SOMO, so that the only contribution to spin densities at nuclei comes from spin polarization. Although this result corresponds to the familiar picture predicted by elementary molecular orbital theory, our study brings additional information. The most striking feature of our computations is that the N and O atoms of the nitroxide groups do not show equal hcc's in the most stable planar conformation. In particular, both N and O atoms belonging to the nitroxide group engaged in the H bond have hcc's significantly larger than those of the free NO moiety. The sp^2 carbon atom bridging the two NO groups (C_2) has the most negative hcc of the whole radical, in agreement with results obtained for other substituted nitronyl nitroxides.[52] The polarization effects, which are responsible for this negative constant, are well evidenced by the different shapes of the unrestricted α and β spin orbitals corresponding to the highest nominally doubly occupied orbital (Figure 7).

A significant variation of the absolute values of the computed hcc's is observed in going from the gas phase to aqueous solution. In particular, a significant decrease of the C_2 hcc's is found (−0.7 G), together with an increase of the N_1 and N_3 constants (0.4 and 0.9 G, respectively). This latter variation is particularly significant because the increase is more important for N_3 than for N_1. As a consequence, the overall effect of the

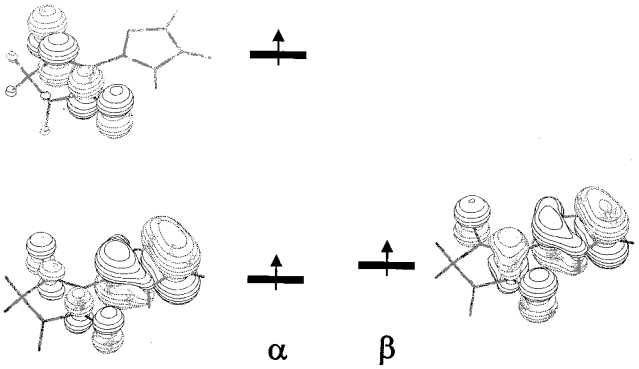

Figure 7. Higher occupied molecular spin orbitals of R2.

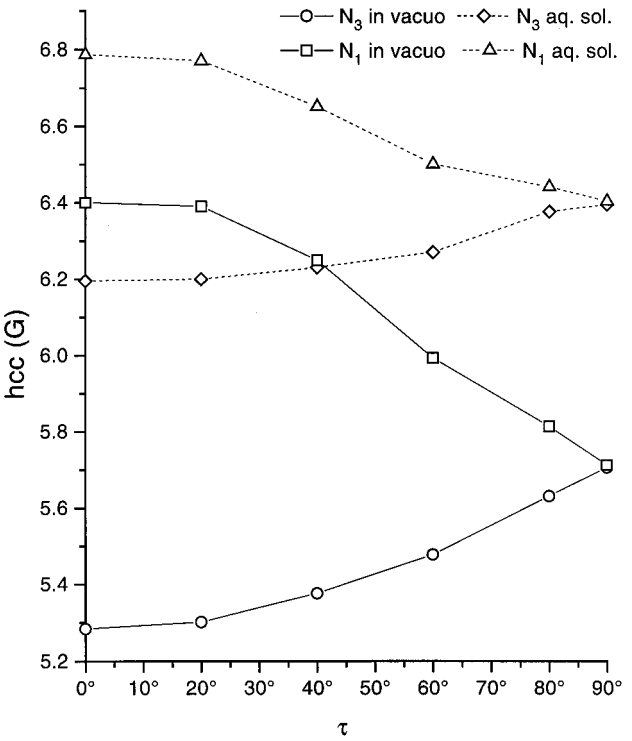

Figure 8. Hyperfine coupling constants (hcc, G) of R2 as funtion of the τ torsional angle. All of the values have been computed at the UB1LYP/EPR-II level, both in vacuo and in aqueous solution.

solvent is to make the two hcc's closer to each other and to the experimental data. In fact, the difference of 1.1 G between both hcc's obtained in vacuo is reduced to 0.6 G in aqueous solution. The effect of the solvent on the hyperfine parameters is further evidenced by the hcc's computed in solution for selected values of the torsional angle τ (see Figure 8).

These plots show the decrease of the N_1 hcc and the corresponding increase of the N_3 hcc as a function of τ, until they reach the same value for $\tau = 90°$. It must be noted, also, that for any value of the torsional angle, the hcc's are always higher in solution than in vacuo.

In summary solvent and, more generally, environmental effects, influence at the same time the structure and electronic properties of R2, inducing two different effects on its magnetic properties. On the one hand, the environment polarizes the radical, thus forcing a significant reorganization of the spin density over the nitronyl moiety. The net effect is a reduction of the difference between the hcc's of the nitroxide groups. On the other hand, the torsional potential of R2 is modified by its environment. Polar solvents and specific intermolecular interactions work cooperatively to decrease the rotational barrier around

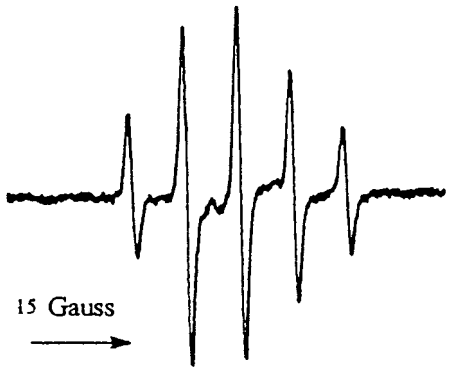

Figure 9. ESR spectrum of R2 in aqueous solution.

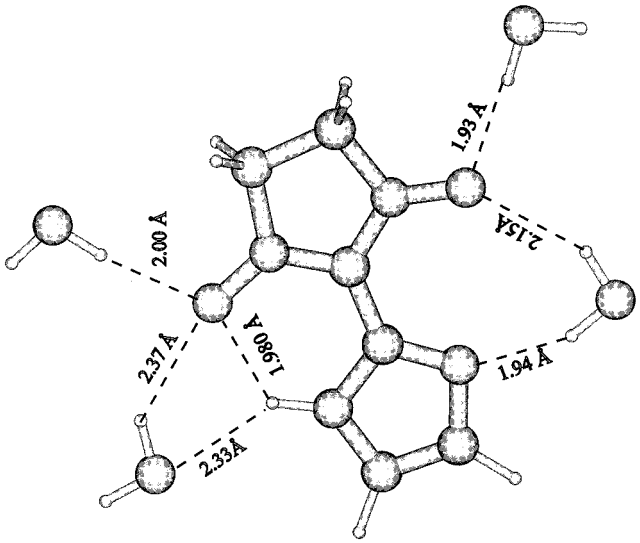

Figure 10. Adduct used for studying specific solvent effects on the hyperfine structure of R2.

the $C_2C_{2'}$ bond, allowing a larger contribution of twisted structures to the observed physicochemical properties. We have taken into account this effect by averaging the hcc's over the torsional motion using a procedure discussed in detail in previous works.[10] Although vibrational averaging is often significant,[10] in the present case the hcc's of nitrogen atoms are modified by less than 0.2 G with respect to their static equilibrium values. As a consequence, our best computations indicate the presence of two ESR signals in solution separated by about 0.5 G, whereas a single average signal should be found in the solid state. In contrast, the ESR spectra recorded in aqueous solution show only one signal at about 7.9 G (7.4 in CH_2Cl_2), which corresponds to both N_1 and N_3 atoms (Table 3 and Figure 9).

One possible explication of this result is that our quantum mechanical computations still overestimate conjugative effects and that in solution the rotation around the $C_2-C_{2'}$ bond is free or, at least, the barrier is so low that the rotation time is shorter than the response of the instrument. On the other hand, specific water molecules bound to the polar atoms of R2 could alter the results predicted by a continuum solvent model. Following previous studies[10] we have therefore optimized, by our nitroxide force field,[46] the intermolecular parameters of the adduct of R2 with four water molecules shown in Figure 10.

Next, hcc's have been computed at the B1LYP level for this supermolecule immersed in a polarizable continuum. The results show that in the present case the continuum model is able to reproduce a significant part of the effect due to strongly bound water molecules, but that the combined discrete−continuum model leads to a further reduction of the asymmetry between nitrogen moieties, which restores full agreement with experiment (see Table 3).

From a more general point of view, the present results are worth being compared with the recently reported spin density distribution in substituted nitronyl nitroxides coordinated to metal ions.[53] In the coordinated species the spin density is unevenly shared by the oxygen and nitrogen atoms of the bound NO group. Depending on the coordination mode and on the magnitude of the metal−nitroxide magnetic interaction, the spin density on the bound oxygen is modified and may completely vanish. In giving comparable populations to both atoms of the NO groups, the present study affords a definite proof of the reorganization of the spin distribution upon coordination and brings strong support to the proposed participation of the ionic Lewis structure of nitroxide groups in metal complexes.

Despite the strong modification of the spin distribution on nitrogen and oxygen atoms, the negative spin density on the sp^2 carbon atoms bridging the NO groups is also present in the coordinated case. The magnitude of this negative population remains equal to approximately one-third of averaged N and O populations, as found in the isolated species. Thus the reorganization of the spin distributions does not affect the polarization of the sp^2 carbon atom.

4. Conclusion

In the present paper we have reported a detailed analysis of the structure and spin-dependent properties of typical nitronyl nitroxide radicals both in vacuo and in condensed phases. This investigation has been carried out using a new powerful computational tool, in which an integrated DFT/post-HF model has been extended to condensed phases taking into the proper account polarization effects. Our results show how subtle effects arising from interaction with the environment tune the conformations and the hyperfine coupling constants, restoring the agreement between computations and experiments.

Together with the specific interest of the free radicals studied in the present work, we think that this kind of integrated approach could be very appealing for the study of large systems both in vacuo and in condensed phases. The more so as even larger compounds can be studied by a three-level procedure in which structural and electrostatic effects of more distant parts are included by a molecular mechanic model.[54,55] We have already extended some last generation force fields to radical systems[46] and integrated the whole PCM/QM/MM model in the development version of the Gaussian system of programs.[56] As a consequence, this kind of study can or will shortly be feasible also for non specialists, thus providing a powerful additional tool for the microscopic interpretation of experimental results, especially when only partial data are available or concurrent interpretation is possible.

Acknowledgment. The authors thank Dr. S. Ohba (Keio University) for providing them crystallographic data. The financial support of the Italian Research Council (CNR) is also gratefully acknowledged.

References and Notes

(1) Rassat, A. *Pure Appl. Chem.* **1990**, *62*, 223.

(2) (a) Capiomont, A.; Lajzerowicz-Bonneteau, J. *Acta Crystallogr.* **1971**, *B27*, 322. (b) Turley, J. W.; Boer, F. P. *Acta Crystallogr.* **1972**, *B28*, 618. (c) Lajzerowicz-Bonneteau, J. In *Spin Labeling, Theory and Applications*; Berliner, D., Ed.; Academic Press: New York, 1970; p 239.

(3) (a) Ricca, A.; Tronchet, J. M.; Weber, J.; Ellinger, Y. *J. Phys. Chem.* **1992**, *96*, 10779. (b) Bordeaux, D.; Boucherle, J. X.; Delley, B.; Gillon,

B.; Ressouche, E.; Schweizer, J. In *Magnetic Molecular Materials*; Gatteschi, D., Kahn, O., Miller, J. S., Palacio, F., Eds.; NATO ASI Series; Kluwer: Dordrecht, 1991; p 371.

(4) (a) Hanson, P.; Lilhauser, G.; Formaggio, F.; Crisma, M.; Toniolo, C. *J. Am. Chem. Soc.* **1996**, *118*, 7618. (b) Keana, J. F. W. *Chem. Rev.* **1978**, *78*, 37.

(5) Janzen, E. G. *Acc. Chem. Res.* **1971**, *4*, 31.

(6) (a) Yamada, B.; Fujita, M.; Otsu, T. *Makromol. Chem.* **1991**, *192*, 1829. (b) Abe, K.; Suezawa, H.; Hirota, M.; Ishii, T. *J. Chem. Soc., Perkin Trans. 2* **1984**, 29.

(7) Tronchet, J. M. In *Bioactive Spin Labels*; Springer-Verlang: Berlin, 1992; p 355.

(8) Caneschi, A.; Gatteschi, D.; Rey, P. *Prog. Inorg. Chem.* **1991**, *39*, 331.

(9) Kahn, O. *Molecular Magnetism*; VCH: New York, 1993.

(10) (a) Rega, N.; Cossi, M.; Barone, V. *J. Chem. Phys.* **1996**, *105*, 11060. (b) Rega, N.; Cossi, M.; Barone, V. *J. Am. Chem. Soc.* **1997**, *119*, 12962; (c) Rega, N.; Cossi, M.; Barone, V. *J. Am. Chem. Soc.* **1998**, *120*, 5723

(11) Barone, V.; Bencini, A.; di Matteo, A. *J. Am. Chem. Soc.* **1997**, *119*, 10831.

(12) Barone, V.; Adamo, C.; Russo, N. *Chem. Phys. Lett.* **1993**, *212*, 5.

(13) Barone, V In *Recent Advances in Density Functional Methods*, Part 1; Chong, D. P., Ed.; World Scientific Publishing Co.: Singapore, 1995; p 287.

(14) Barone, V. *Chem. Phys. Lett.* **1996**, *262*, 201.

(15) Adamo, C.; Barone, V.; Fortunelli, A. *J. Chem. Phys.* **1995**, *102*, 384.

(16) Boesch, S. E.; Wheeler, R. A. *J. Phys. Chem. A* **1997**, *101*, 5799.

(17) Noodleman, L.; Peng, C. Y.; Case, D. A.; Mouesca, J. M. *Coord. Chem. Rev.* **1995**, *144*, 199.

(18) Bencini, A.; Totti, F.; Daul, C. A.; Doclo, K.; Fantucci, P.; Barone, V. *Inorg. Chem.* **1997**, *36*, 5022.

(19) Erickson, L. A.; Malkin, V. G.; Malkina, O. L.; Salahub, D. R. *J. Chem. Phys.* **1993**, *217*, 24

(20) O'Malley, P. J. *J. Phys. Chem. A* **1998**, *102*, 248.

(21) Himo, F.; Graslund, A.; Eriksson, L. A.; *Biophys. J.* **1997**, 72, 1556.

(22) Jolibois, F.; Cadet, J.; Grand, A.; Subra, R.; Rega, N.; Barone, V. *J. Am. Chem. Soc.* **1998**, *120*, 1864.

(23) Adamo, C.; Barone, V. *Chem. Phys. Lett.* **1997**, *274*, 242.

(24) Adamo, C.; Barone, V. *J. Chem. Phys.* **1998**, *108*, 664.

(25) Adamo, C.; Barone, V.; Bencini, A.; Ciofini, I.; Daul, C. A.; Totti, F. *Inorg.Chem.*, in press.

(26) Amovilli, C.; Barone, V.; Cammi, R.; Cancés, R.; Cossi, M.; Mennucci, B.; Pomelli, C. S.; Tomasi, J. *Adv. Quantum Chem.* **1998**, *32*, 227.

(27) (a) Cossi, M.; Barone, V.; Cammi, R.; Tomasi, J. *Chem. Phys. Lett.* **1996**, *255*, 327. (b) Cossi, M., Barone,V. *J. Phys. Chem. A* **1998**, *102*, 1995. Cossi, M., Barone, V. *J. Chem. Phys.* **1998**, 109, 6246. (c) Klamt, A.; Schüürmann, A. G. *J. Chem. Soc., Perkin Trans. 2* **1993**, 799. Klamt, A.; Jonas, V. *J. Chem. Phys.* **1996**, *105*, 9972. Balldridge, K.; Klamt, A. *J. Chem. Phys.* **1997**, *106*, 6622.

(28) Frisch, M. J.; Trucks, G. W.; Schlegel, H. B.; Scuseria, G. E.; Stratmann, R. E.; Burant, J. C.; Dapprich, S.; Millam, J. M.; Daniels, A. D.; Kudin, K. N.; Strain, M. C.; Farkas, O.; Tomasi, J.; Barone, V.; Cossi, M.; Cammi, R.; Mennucci, B.; Pomelli, C.; Adamo C.; Clifford, S.; Ochterschi, J.; Cui, Q.; Gill, P. M. W.; Johnson, B. G.; Robb, M. A.; Cheeseman, J. R.; Keith, T.; Petersson, G. A.; Morokuma, K.; Malick, D. K.; Rabuck, A. D.; G. A.; Montgomery, J. A.; Raghavachari, K.; Al-Laham, M. A.; Zakrewski, V. G.; Ortiz, J. V.; Foresman, J. B.; Cioslowski, J.; Stefanov, B. B.; Nanayakkara, A.; Liu, J.; Liashenklo, A.; Piskorz, P.; Komaromi, I.; Challacombe, M.; Peng, C. Y.; Ayala, P. Y.; Chen, W.; Wong, M. W.; Andres, J. L.; Replogle, E. S.; Gomperts, R.; Martin, R. L.; Fox, D. J.; Binkley, J. S.; DeFrees, D. J.; Baker, J.; Stewart, J. P.; Head-Gordon, M.; Gonzalez, C.; Pople. J. A. *Gaussian 98 (Revision A.5)*; Gaussian Inc.: Pittsburgh, PA, **1998**.

(29) Yoshioka, N.; Irisawa, M.; Mochozuki, Y.; Kato, T.; Inoue, H.; Ohba, S. *Chem. Lett.* **1997**, 251.

(30) Karpfen, A.; Ho Choi, C.; Kertesz, M. *J. Phys. Chem. A* **1997**, *101*, 7426.

(31) Fegy, K.; Sanz, N.; Luneau, D.; Belorizky, E.; Rey, P., in press.

(32) Ullman, A. F.; Osiecki, J. H.; Boocock, D. G. B.; Darcy, R. *J. Am. Chem. Soc.* **1972**, *94*, 7049.

(33) Luneau, D.; Rey, P.; Laugier, J.; Beloritzky, E.; Cogne, A. *Inorg. Chem.* **1992**, *31*, 3578.

(34) Becke, A. D.; *Phys. Rev. B* **1988**, *38*, 3098.

(35) Lee, C.; Yang, W.; Parr, R. G. *Phys. Rev. B* **1988**, *37*, 785.

(36) Krishnan, R.; Binkley, J. S.; Seeger, R.; Pople, J. A. *J. Chem. Phys.* **1980**, *72*, 650.

(37) Barone, V. *J. Phys. Chem.* **1995**, *99*, 11659.

(38) A description of standard basis sets and levels of theory can be found in Foresman, J. B.; Frisch, A. E. *Exploring Chemistry with Electronic Structure Methods*, 2nd ed.; Gaussian Inc.: Pittsburgh, PA, 1996.

(39) (a) Sekino, H.; Bartlett, R. J. *J. Chem. Phys.* **1985**, *82*, 4225. (b) Pereira, S. A.; Watts, J. D.; Bartlett, R. J. *J. Chem. Phys.* **1994**, *100*, 1425.

(40) (a) Barone, V.; Minichino, C.; Grand, A.; Subra, R. *J. Chem. Phys.* **1993**, *99*, 6787. (b) Barone, V.; Subra, R. *J. Chem. Phys.* **1996**, *104*, 2630. (c) Barone, V.; Adamo, C.; Brunel, Y.; Subra, R. *J. Chem. Phys.* **1996**, *105*, 3168.

(41) Weltner, W., Jr. *Magnetic Atoms and Molecules*; Dover: New York, 1989.

(42) Barone, V.; Cossi, M.; Tomasi, J. *J. Chem. Phys.* **1997**, *107*, 3210.

(43) Wang, J.; Becke, A. D.; Smith V. H., Jr. *J. Chem. Soc.* **1995**, *102*, 3477.

(44) Cogne, A.; Grand, A.; Rey, P.; Subra, R. *J. Am. Chem. Soc.* **1989**, *111*, 3220.

(45) Barone V.; Grand, A.; Luneau, D.; Rey, P.; Minichino, C.; Subra, R.; *New. J. Chem.* **1993**, *17*, 1587.

(46) Barone, V.; Bencini, A.; Cossi, M.; di Matteo, M.; Mattesini, M.; Totti, F. *J. Am. Chem. Soc.* **1998**, *120*, 7069.

(47) D'Anna, J. A.; Wharton, J. H. *J. Chem. Phys.* **1970**, *53*, 4047.

(48) Barone, V. *Chem. Phys. Lett.* **1996**, *262*, 201.

(49) Zheludev, A.; Barone V.; Boumet, M.; Delley, B.; Grand, A.; Ressouche, E.; Rey, P.; Subra, R.; Schweizer, J. *J. Am. Chem. Soc.* **1994**, *116*, 2019.

(50) Ohba, S., private communication.

(51) (a) Barone, V.; Lelj, F.; Russo, N. *Int. J. Quantum Chem.* **1986**, *29*, 541. (b) Barone, V.; Minichino, C.; Fliszar, S.; Russo, N. *Can. J. Chem.* **1988**, *66*, 1313.

(52) Rey, P., unpublished results.

(53) Ressouche, E.; Boucherle, J. X.; Gillon, B.; Rey, P.; Schweizer, J. *J. Am. Chem. Soc.* **1993**, *115*, 3610.

(54) Svensson, M.; Humbel, S.; Froese, R. D. J.; Matsubara, T.; Sieber, S.; Morokuma, K. *J. Phys. Chem.* **1996**, *100*, 19357.

(55) Dapprich, S.; Komaromi, I.; Byun, K.S.; Morokuma, K.; Frisch, M. J. *Theor. Chem. Acc.*, in press.

(56) Cossi, M.; Barone, V., in preparation.